# Influence of Electron-Withdrawing Substituents on the Electronic Structure of Oxidized Ni and Cu Salen Complexes

Linus Chiang,[†] Khrystyna Herasymchuk,[†] Fabrice Thomas,[§] and Tim Storr*,[†]

[†]Department of Chemistry, Simon Fraser University, Burnaby, British Columbia V5A 1S6, Canada

[§]Département de Chimie Moléculaire, Chimie Inorganique Redox (CIRE), UMR-5250, Université Grenoble Alpes, BP 53, 38041 Grenoble Cedex 9, France

S *Supporting Information*
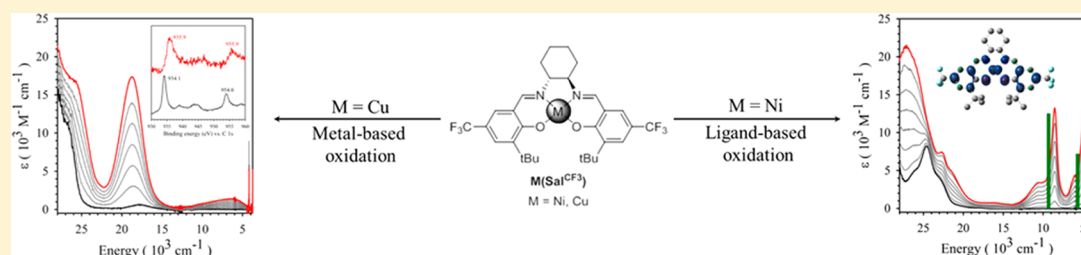
ABSTRACT: Nickel ($Ni(Sal^{CF3})$) and copper ($Cu(Sal^{CF3})$) complexes of an electron-poor salen ligand were prepared, and their one-electron oxidized counterparts were studied using an array of spectroscopic and theoretical methods. The electrochemistry of both complexes exhibited quasi-reversible redox processes at higher potentials in comparison to the $M(Sal^R)$ (R = ^tBu, OMe, NMe_2) analogues, in line with the electron-withdrawing nature of the *para*-CF_3 substituent. Chemical oxidation, monitored by ultraviolet−visible−near-infrared (UV−vis−NIR) spectroscopy, afforded their corresponding one-electron oxidized products. Ligand-based oxidation was observed for $[Ni(Sal^{CF3})]^{+\bullet}$, as evidenced by sharp NIR transitions in the UV−vis−NIR spectrum and a broad isotropic signal at $g = 2.067$ by solution electron paramagnetic resonance (EPR) spectroscopy. Such sharp NIR transitions observed for $[Ni(Sal^{CF3})]^{+\bullet}$ are indicative of a delocalized electronic structure, which is in good agreement with electrochemical measurements and density functional theory (DFT) calculations. In addition, the increased Lewis acidity of $[Ni(Sal^{CF3})]^{+\bullet}$, evident from the EPR g-value and DFT calculations, was further quantified by the binding affinity of axial ligands to $[Ni(Sal^{CF3})]^{+\bullet}$. For $[Cu(Sal^{CF3})]^+$, an intense ligand-to-metal charge transfer band at 18 700 cm^{-1} in the UV−vis−NIR spectrum was observed, which is diagnostic for the formation of a Cu^{III} species [*J. Am. Chem. Soc.*, **2008**, *130*, 15448−15459]. The Cu^{III} character for $[Cu(Sal^{CF3})]^+$ is further confirmed by ^{19}F NMR analysis. Taken together, these results show that the electron-deficient salen ligand H_2Sal^{CF3} increases the Lewis acidity of the coordinating metal center.

1. INTRODUCTION

Transition metal complexes incorporating redox-active ligands are of significant current interest,[1] drawing inspiration from enzymatic systems such as galactose oxidase[2] and cytochrome P450.[3] Reports have documented the pro-radical nature of ligands such as dioxolenes,[4] dithiolenes,[5] phenolates,[2b,6] *o*-phenylenediamines,[7] amidophenolates,[8] 1,2-diimines,[9] and salens.[1a] This research has greatly improved our understanding of the interaction between transition metal ions and pro-radical ligands and has stimulated transition metal catalyst development incorporating redox-active ligands.[1,8b,c,9i,10]

The relative ordering of the metal and ligand frontier orbitals dictates whether a metal complex (M^nL) will become a ligand-radical complex ($[M^{n+}L^{\bullet}]^+$) or a high-valent metal complex ($[M^{(n+1)}L]^+$) upon oxidation. Minor changes to the system through solvent/temperature variations or addition of exogenous ligands is sufficient in shifting the locus of oxidation in certain cases.[4,11] One area of recent focus by our group and others is the redox activity and electronic structure of tetradentate salen (**Sal**) ligands (salen is a common

abbreviation for N_2O_2 bis-Schiff-base bis-phenolate ligands).[2b,12] Salen ligands have been extensively studied due to their modular synthesis, ability to stabilize many metals in different oxidation states, and versatility as catalysts.[13] As an example, one-electron oxidized $Ni^{II}(Sal)$ derivatives exist in the ligand radical form $[Ni^{II}(Sal^{\bullet})]^+$ in solution and the solid state, where ligand electronic tuning via *para*-ring substituent variation influences the degree of delocalization of the ligand radical.[12c] The addition of exogenous ligands such as dimethylformamide (DMF) or pyridine to $[Ni^{II}(Sal^{\bullet})]^+$ results in the shifting of the oxidation locus to the octahedral $[Ni^{III}(Sal)(D)_2]^+$ form (D = axial donor ligand).[12g,n,q,14] Recent work on $Co^{II}(Sal)$ systems has shown that the relative donating abilities of the axial ligands dictates the formation of $[Co^{II}(Sal^{\bullet})(D)_x]^+$ or $[Co^{III}(Sal)(D)_x]^+$ (x = 1 or 2).[12s,15]

In this work, we investigate the electronic structure of oxidized nickel ($Ni(Sal^{CF3})$) and copper ($Cu(Sal^{CF3})$)

complexes with electron-withdrawing CF_3 substituents in the *para* position (Chart 1) to determine if electron-withdrawing

Chart 1. Nickel ($Ni(Sal^{CF3})$) and Copper ($Cu(Sal^{CF3})$) Complexes

$M(Sal^{CF3})$
M = Ni, Cu

moieties promote metal-based versus ligand-based oxidation. Because of the geometric preferences of Ni and Cu, the factors governing the locus of oxidation differ. For example, while Ni^{III} d^7 complexes are usually stabilized in an octahedral environment, a square-planar ligand geometry is much preferred for Cu^{III} complexes. Previous research focusing on square-planar $Ni^{II}(Sal^R)$ complexes found that the use of electron-donating *para*-ring substituents (i.e. ^tBu, SR, OMe, NMe_2) promotes ligand radical formation at low oxidation potentials.[12c,o] Interestingly, oxidation of four-coordinate square-planar Ni^{II} complexes employing diamido-diphenolate ligands,[16] *o*-phenyl-enedioxamides and related ligands,[15c,17] and dipeptides[18] afford Ni^{III} species likely due to the tetra-anionic nature of the ligands. Will dianionic $M(Sal^{CF3})$ complexes also support a Ni^{III} oxidation state in a square-planar ligand environment?

For Cu, the majority of Cu^{III} complexes reported employ anionic ligands such as carboxylates, thiolates, deprotonated amides, carbamates, and N-confused porphyrins. Recent interest in the stabilization of Cu^{III} complexes arises from the isolation of Cu^{III} intermediates in organocopper chemistry[19] and from the synthesis and reactivity of bis(μ-oxo)dicopper-(III) complexes.[20] Oxidation of the $Cu^{II}(Sal^R)$ system employing ^tBu *para*-ring substituents affords a Cu^{III} complex in the solid state, yet in solution a reversible spin-equilibrium exists between the ligand radical species $[Cu^{II}(Sal^\bullet)]^+$ and high-valent metal form $[Cu^{III}(Sal)]^+$.[12f] Employing OMe *para*-ring substituents, however, affords a ligand radical species upon oxidation under all conditions investigated.[12q] These studies highlight the effect of salen ligand electronics in dictating the electronic structure of their oxidized forms. Herein, we describe the electronic structure of oxidized $M(Sal^{CF3})$ (M = Ni, Cu) using experimental and theoretical methods. Oxidized $[Ni-(Sal^{CF3})]^{+\bullet}$ is demonstrated to exist as a delocalized ligand radical with considerable metal ion participation in the singularly occupied molecular orbital (SOMO), while oxidized $[Cu(Sal^{CF3})]^+$ exists as a Cu^{III} complex in solution and in the solid state.

2. EXPERIMENTAL SECTION

2.1. Materials and Methods. All chemicals used were of the highest grade available and were further purified whenever necessary.[21] 2-*tert*-butyl-4-trifluoromethyl phenol was prepared from commercially available 4-trifluoromethyl phenol by reported procedures.[22] The tris(2,4-dibromophenyl)aminium hexafluoroantimonate radical chemical oxidant $N(C_6H_3Br_2)_3SbF_6$ ($E_{1/2}$ = 1.14 V, MeCN)[23] was synthesized according to published protocols.[14,24] Electronic spectra were obtained on a Cary 5000 spectrophotometer with a custom-designed immersion fiber-optic probe with variable path length (1 and 10 mm; Hellma, Inc.). Constant temperatures were maintained by a

dry ice/acetone bath. Solvent contraction was accounted for in all variable-temperature studies. Affinity constants were obtained by refinement of the UV−vis titration data of the complexes with pyridine in CH_2Cl_2. Data fitting was completed using SPECFIT software. Cyclic voltammetry (CV) was performed on a PAR-263A potentiometer, equipped with a Ag wire reference electrode, a platinum disk working electrode, and a Pt counter electrode with $^nBu_4NClO_4$ (0.1 M) solutions in CH_2Cl_2. Decamethylferrocene was used as an internal standard.[25] ^1H, ^{13}C, and ^{19}F NMR spectra were recorded on a Bruker AV-500 instrument. Mass spectra (electrospray ionization (ESI) positive ion or ESI negative ion) were obtained on an Agilent 6210 TOF ESI-MS instrument. Elemental analyses (C, H, N) were performed by Mr. P. Mulyk at Simon Fraser University on a Carlo Erba EA1110 CHN elemental analyzer. All electron paramagnetic resonance (EPR) spectra were collected using a Bruker EMXplus spectrometer operating with a premiumX X-band (~9.5 GHz) microwave bridge. Low-temperature measurements of frozen solutions used a Bruker helium temperature-control system and a continuous-flow cryostat. Samples for X-band measurements were placed in 4 mm outer-diameter sample tubes with sample volumes of ~300 μL. Spectra at 195 K were collected in capillary tubes, which were placed inside a standard 4 mm EPR tube.

2.2. X-ray Structure Determination. Single crystal X-ray crystallographic analysis of $Ni(Sal^{CF3})$ and $Cu(Sal^{CF3})$ was performed on a Bruker X8 APEX II diffractometer with graphite monochromated Mo Kα radiation. An orange block ($Ni(Sal^{CF3})$) or a dark purple prism ($Cu(Sal^{CF3})$) crystal was mounted on a glass fibre. The data were collected at 150 ± 0.1 K to a maximum 2θ value of 55.0°. Data were collected in a series of ϕ and ω in 0.50° widths with 10.0 s exposures. The crystal-to-detector distance was 50 mm. The structure was solved by direct methods (SIR92)[26] and refined by least-squares procedures using CRYSTALS (v14.40b)[27] or ShelXle.[28] All non-hydrogen atoms were refined anisotropically. All C−H hydrogen atoms were placed in calculated positions but were not refined. All crystal structure plots were produced using ORTEP-3 and rendered with POV-Ray (v.3.6.2). A summary of the crystal data and experimental parameters for structure determinations are given in Table 1.

2.3. Oxidation Protocol. Under an inert atmosphere at 195 K, 500 μL of a CH_2Cl_2 solution of the metal complex (4.6 mM) was added to 3.0 mL of CH_2Cl_2. Monitored by UV−vis−NIR spectroscopy, a saturated solution of $N(C_6H_3Br_2)_3SbF_6$ in CH_2Cl_2 was added in 60 μL aliquots resulting in clean conversion to the respective one-electron oxidized species.

Table 1. Selected Crystallographic Data for $Cu(Sal^{CF3})$

complex	$Cu(Sal^{CF3})$
formula	$C_{30}H_{34}F_6N_2O_2Cu$
formula weight	632.14
space group	$P2_1/n$
a (Å)	8.3007(7)
b (Å)	17.9066(14)
c (Å)	19.9819(16)
α (deg)	90
β (deg)	98.9040(15)
γ (deg)	90
V [Å^3]	2934.3(4)
Z, D_{calc} [g/cm^3]	4
T (K)	150
ρ_{calcd} (g cm^{-3})	1.431
λ (Å)	0.710 73
μ (cm^{-1})	0.812
R indices^a with $I > 2\sigma(I)$ (data)	5351
wR_2	0.1626
R_1	0.0440
goodness-of-fit on F^2	1.509

^{a}Goodness-of-fit on F.

2.4. X-ray Photoelectron Spectroscopy. Solid samples of the oxidized species were prepared under an inert atmosphere. The oxidized samples were prepared by dissolving the neutral compounds in CH$_2$Cl$_2$, then cooled to 233 K, when N(C$_6$H$_3$Br$_2$)$_3$SbF$_6$ was added in one portion. Solvent was immediately evacuated, where the color between the solution and resultant solid was maintained. X-ray photoelectron spectra were obtained using a Kratos Analytical Axis ULTRA spectrometer containing a DLD detector. The solid samples were loaded onto the carbon tape under inert atmosphere, and the auto-z correction was done using F(1s) binding energy. The X-ray excitation source was at 15 kV and 10 mA. All spectra were referenced to the C(1s) peak (284.2 eV).

2.5. Calculations. Geometry optimizations were performed using the Gaussian 09 program (Revision D.01),[29] the B3LYP[30] functional with a polarized continuum model (PCM) for CH$_2$Cl$_2$ (dielectric ε = 8.94),[31] and the 6-31G(d) basis set on all atoms. This combination of functional and basis set has been used previously for structurally similar salen complexes, providing good matches to experimental metrical parameters.[12b,d,e] A symmetric structure was used as a starting point for all geometry optimizations. Frequency calculations at the same level of theory confirmed that the optimized structures were located at a minimum on the potential energy surface. Single point calculations for the Ni complexes were performed using the B3LYP[30] functional with a PCM for CH$_2$Cl$_2$,[31] and the TZVP basis set of Ahlrichs on all atoms.[32] The intensities of the 30 lowest-energy electronic transitions for [Ni(Sal^{CF3})]$^{+\bullet}$ were calculated by time-dependent density functional theory (TD-DFT)[33] at the B3LYP/TZVP level with a PCM for CH$_2$Cl$_2$. The above calculations were also completed using the CAM-B3LYP[34] functional for comparison. Single point calculations for energetic analysis of the Cu complexes were performed using the BLYP[35] functional with a PCM for CH$_2$Cl$_2$,[31] and the TZVP basis set of Ahlrichs on all atoms.[32] AOMix[36] was used for determining atomic orbital compositions employing Mulliken Population Analysis.

2.6. Synthesis. *2.6.1. 3-tert-Butyl-5-trifluoromethylsalicyl-aldehyde (1).* To a solution of 2-*tert*-butyl-4-trifluoromethyl phenol (1.5 g, 6.9 mmol) in trifluoroacetic acid (30 mL) was added hexamethylenetetramine (1.06 g, 7.6 mmol). The reaction mixture was stirred at reflux for 16 h; then it was cooled to room temperature, and water (30 mL) was added. This solution was cooled and extracted with CH$_2$Cl$_2$ (3 × 50 mL), the organic phase was dried over Na$_2$SO$_4$, and the filtrate was concentrated in vacuo. The crude product was subject to flash column chromatography using 4:1 CHCl$_3$/hexanes as the eluent to afford a pale yellow oil as 3-*tert*-butyl-5-trifluoromethylsalicylaldehyde. Yield: 430 mg, 25%. ^{1}H NMR (CDCl$_3$, 400 MHz): δ = 12.11 (s, 1H, OH), 9.92 (s, 1H, CHO), 7.71−7.70 (m, 2H, Ar−H), 1.44 (s, 9H, ^{t}Bu); ^{13}C NMR (CDCl$_3$, 100 MHz): δ = 196.7, 163.7, 140.0, 130.5 (^3J(C,F) = 3 Hz), 129.4 ($^3J_{C−F}$ = 4 Hz), 124.0 (^1J(C,F) = 271 Hz), 121.8 (^2J(C,F) = 33 Hz), 119.9, 35.3, 29.1. MS (ESI negative mode): m/z (%): 245.08 (100) [**1**+H]$^+$.

2.6.2. (N,N'-Bis(3-tert-butyl-5-trifluoromethylsalicylidene))-trans-1,2-cyclohexanediamine (H$_2$(Sal^{CF3})). To a solution of *trans*-1,2-cyclohexanediamine (71 mg, 0.6 mmol) dissolved in MeOH (3 mL) was added 3-*tert*-butyl-5-trifluoromethyl-2-hydroxybenzaldehyde (305 mg, 1.2 mmol) in MeOH (3 mL). The reaction mixture was stirred at room temperature for 16 h, during which time a light yellow precipitate formed. The solid was filtered and washed with cold MeOH. Yield: 330 mg (93%). ^{1}H NMR (CDCl$_3$): δ = 8.30 (s, 2H, NCH), 7.44−7.45 (d, 2H, Ar−H, J = 2.0 Hz), 7.25−7.26 (d, 2H, Ar−H, J = 2.0 Hz), 3.35−3.42 (m, 2H, CH), 2.02−2.05 (m, 2H, CH$_2$), 1.88−1.96 (m, 2H, CH$_2$), 1.74−1.82 (m, 2H, CH$_2$), 1.45−1.55 (m, 2H, CH$_2$), 1.40 (s, 18H, ^{t}Bu). ^{13}C NMR (CDCl$_3$, 100 MHz): δ = 165.1, 163.2, 138.7, 127.0, ($^3J_{C−F}$: 4 Hz), 126.2 ($^3J_{C−F}$: 3 Hz), 124.5 (CF$_3$, $^2J_{C−F}$: 271 Hz), 120.0, 117.8, 72.3, 35.1, 32.9, 29.1, 24.3; ^{19}F NMR (CDCl$_3$, 560 MHz): δ = −62.8. MS (ESI): m/z (%): 571.27 (100) [**H$_2$(Sal^{CF3})**+H]$^+$. Anal. Cald (%) for C$_{30}$H$_{36}$N$_2$O$_2$F$_6$: C 63.15, H 6.36, N 4.91; Found (%): C 63.50, H 6.53, N 5.12.

2.6.3. (N,N'-Bis(3-tert-butyl-5-trifluoromethylsalicylidene))-trans-1,2-cyclohexanediamine Nickel(II) (Ni(Sal^{CF3})). To a solution of **H$_2$(Sal^{CF3})** (50 mg, 0.09 mmol) in Et$_2$O (2 mL) was added Ni(OAc)$_2$·

4H$_2$O (22 mg, 0.09 mmol) in MeOH (2 mL). NEt$_3$ (25 µL, 0.18 mmol) was added, and the resulting solution was stirred at room temperature overnight, during which time an orange precipitate formed, which was collected by filtration and washed with cold methanol. The crude material was recrystallized in 1:1 CH$_2$Cl$_2$/MeOH to afford orange crystals of **Ni(Sal^{CF3})**. Yield: 22 mg (40%). ^{19}F NMR (CDCl$_3$, 560 MHz): δ = −62.5. MS (ESI): m/z (%): 627.20 (100) [**Ni(Sal^{CF3})** + H]$^+$. Anal. Cald (%) for C$_{30}$H$_{34}$N$_2$O$_2$F$_6$Ni: C 57.44, H 5.46, N 4.47; Found (%): C 57.82, H 5.19, N 4.54.

2.6.4. (N,N'-Bis(3-tert-butyl-5-trifluoromethylsalicylidene))-trans-1,2-cyclohexanediamine Copper(II) (Cu(Sal^{CF3})). To a solution of **H$_2$(Sal^{CF3})** (100 mg, 0.18 mmol) in MeOH (2 mL) was added Cu(OAc)$_2$·H$_2$O (35 mg, 0.18 mmol) in MeOH (2 mL). The resulting solution was stirred at room temperature overnight, during which time a dark purple precipitate formed, which was collected by filtration and washed with cold methanol. The crude material was recrystallized in 1:1 CH$_2$Cl$_2$/MeOH to afford dark purple crystals. Yield: 60 mg (54%). ^{19}F NMR (CDCl$_3$, 560 MHz): δ = −64.4. MS (ESI): m/z (%): 632.19 (100) [**Cu(Sal^{CF3})** + H]$^+$. Anal. Cald (%) for C$_{30}$H$_{34}$N$_2$O$_2$F$_6$Cu: C 57.00, H 5.42, N 4.43; Found (%): C 57.09, H 5.39, N 4.64.

3. RESULTS AND ANALYSIS

3.1. Synthesis and Solid State Characterization of Ligands and Complexes. The ligand **H$_2$Sal^{CF3}** was synthesized by condensation of *trans*-1,2-cyclohexanediamine in the presence of 2 equiv of 3-*tert*-butyl-5-trifluoromethyl-2-hydroxybenzaldehyde, which was prepared by the *tert*-butylation of the commercially available 4-trifluoromethylphenol, followed by a Duff formylation reaction. **Ni(Sal^{CF3})** and **Cu(Sal^{CF3})** were synthesized by reacting **H$_2$(Sal^{CF3})** with the corresponding metal acetate salts (Ni(OAc)$_2$·4H$_2$O and Cu(OAc)$_2$·4H$_2$O) under aerobic conditions (Scheme 1).

Scheme 1. Synthetic Scheme for H$_2$(Sal^{CF3}) and M(Sal^{CF3})^a
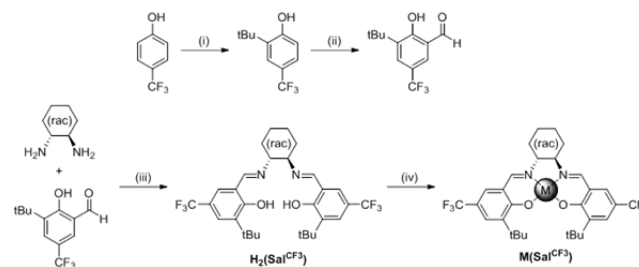
^{a}(i) 9:1 ^{t}BuOH/MeOH, H$_2$SO$_4$, 74%; (ii) hexamethylenetetramine, CF$_3$COOH, 25%; (iii) 0.5 equiv *trans*-1,2-cyclohexanediamine, MeOH, 93%; (iv) M(OAc)$_2$, MeOH, Ni: 40%, Cu: 54%.

NEt$_3$ (2 equiv) was added to all metallation reactions. X-ray quality crystals of **Ni(Sal^{CF3})** and **Cu(Sal^{CF3})** were grown by slow diffusion of MeOH into a concentrated CH$_2$Cl$_2$ solution of the compounds.

3.2. X-ray Analysis of Ni(Sal^{CF3}) and Cu(Sal^{CF3}). The molecular structures of **Ni(Sal^{CF3})** and **Cu(Sal^{CF3})** are presented in Supporting Information, Figure S1 and Figure 1, respectively, and select crystallographic data for **Cu(Sal^{CF3})** are shown in Table 1. A high R value (11.1%) for the X-ray data of **Ni(Sal^{CF3})** arises from a second disordered molecule of **Ni(Sal^{CF3})** in the unit cell, and thus bond lengths could not be accurately determined. The solid-state structure for the two compounds exhibits a slightly distorted square-planar geometry with the expected N$_2$O$_2$ coordination sphere from the ligand, with the distortion likely due to the sterically demanding *ortho*-^{t}Bu substituents. The C−O bond length of the phenolate is often used to evaluate the oxidation state of the ligand.
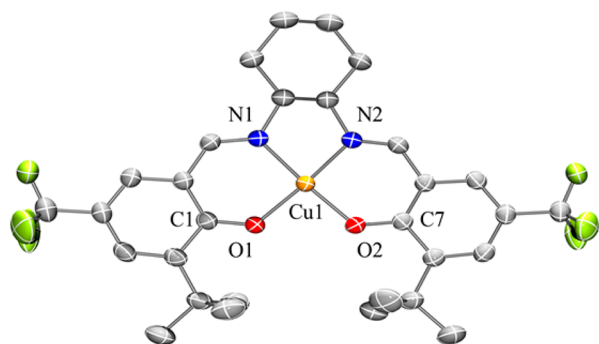
Figure 1. ORTEP plot of **Cu(Sal^{CF3})** (50% probability) using POV-Ray, excluding hydrogen atoms. Selected interatomic distances [Å] and angles [deg]: Cu(1)−N(1): 1.938, Cu(1)−N(2): 1.939, Cu(1)−O(1): 1.901, Cu(1)−O(2): 1.895, C(1)−O(1): 1.295, C(7)−O(2): 1.297; N(1)−Cu(1)−N(2): 84.2, N(2)−Cu(1)−O(2): 93.2, O(1)−Cu(1)−O(2): 90.6, N(1)−Cu(1)−O(1): 92.7, N(1)−Cu(1)−O(2): 173.4, O(1)−Cu(1)−N(2): 172.5.

Cu(Sal^{CF3}) displayed C−O bond distances consistent with a phenolate moiety, in line with other **Cu(Sal^R)** complexes,[12q,37] indicating the dianionic nature of the complex. Overall, the coordination sphere bond distances for **Cu(Sal^{CF3})** were found to be slightly longer in comparison to other reported **Cu(Sal^R)** derivatives, suggesting phenolates bearing the CF$_3$ moiety have lower donating ability in comparison to analogues with a para-^{t}Bu group. This is further illustrated by the shorter coordination bond distances for salen complexes with an electron-rich OMe para-ring substituent, in comparison to the ^{t}Bu analogue.[12q]

3.3. Electrochemistry. Redox processes for **M(Sal^{CF3})** were probed by cyclic voltammetry (CV) in CH$_2$Cl$_2$ by using tetra-n-butylammonium perchlorate (^{n}Bu$_4$NClO$_4$) as the supporting electrolyte. Two quasi-reversible one-electron oxidation waves are observed for **Ni(Sal^{CF3})** as previously observed for other **Ni(Sal^R)** complexes (Figure 2, Table 2).[12c,38]
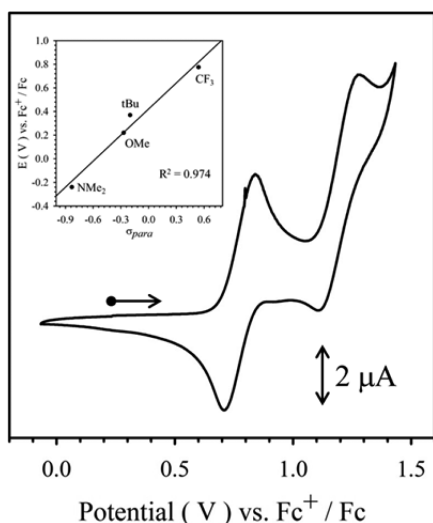
Figure 2. Cyclic voltammogram of **Ni(Sal^{CF3})**. (inset) Hammett plot of the oxidation potentials of **Ni(Sal^R)** vs σ_{para} of the para-ring substituents. Conditions: 1.5 mM complex, 0.1 M ^{n}Bu$_4$NClO$_4$, scan rate 100 mV s^{-1}, CH$_2$Cl$_2$, 298 K.

The redox potentials for **Ni(Sal^R)** versus Fc$^+$/Fc are in line with the electron-donating abilities of the para-ring substituents,[12c] which is reflected in the plot between first oxidation potential against Hammett constants (σ_{para}).[39] A linear correlation ($R^2 = 0.974$) demonstrates that the oxidation potential is predominantly affected by the relative donating ability of the para-ring substituents (Figure 2 inset). Both the first and second redox processes for **Ni(Sal^R)** vary by ca. 1 V in the series (Table 2). In addition, the difference between the first and second oxidation potentials ($\Delta E_{1/2}$) and comproportionation constant (K_c) of the one-electron oxidized complexes, calculated using eqs 1−3, are also reported in Table 2, which provides insight regarding the degree of electronic coupling between the two redox-active phenolates in $[\mathbf{Ni(Sal^{CF3})}]^{+\bullet}$.[40] Both $\Delta E_{1/2}$ and K_c values for $[\mathbf{Ni(Sal^{CF3})}]^{+\bullet}$ suggest a delocalized ligand-radical electronic structure, which is further supported by theoretical analysis (vide supra).

$$[ML] + [ML^{\bullet\bullet}] \leftrightarrow 2[ML^{\bullet}] \tag{1}$$

$$K_c = \frac{[ML^{\bullet}]^2}{[ML][ML^{\bullet\bullet}]} \tag{2}$$

$$K_c = \exp\left(\frac{\Delta E_{ox}F}{RT}\right) \tag{3}$$

Two quasi-reversible one-electron oxidation waves were observed for **Cu(Sal^{CF3})** (Table 3, Supporting Information, Figure S2). The redox processes for **Cu(Sal^{CF3})** occur at considerably higher potentials in comparison to **Cu(Sal^{tBu})** and **Cu(Sal^{OMe})**,[12q,37] as expected based on the trends observed for **Ni(Sal^R)**.[12c] Interestingly, it has been reported that the one-electron oxidation of **Cu(Sal^{tBu})** affords a Cu^{III} species in the solid state, which is in equilibrium with a Cu^{II}-phenoxyl radical species in solution.[12f] The locus of oxidation is strongly dependent on temperature, highlighting the similarity in energy between the two electronic states. Conversely, the one-electron oxidation of the more electron-rich OMe derivative **Cu(Sal^{OMe})** results in a Cu^{II}-phenoxyl radical species at all temperatures.[12q] Thus, the electron-withdrawing properties of the CF$_3$ moiety is expected to lower the energy of the ligand-based highest occupied molecular orbital, thereby stabilizing the formation of a Cu^{III} species (vide infra). In addition, an irreversible reduction wave was observed at −2.06 V in the CV spectrum; similar reduction processes have been observed for other Cu^{II}−Schiff base complexes indicating reduction to their respective Cu^I forms.[41] Similar to the oxidation processes, the para-ring substituents in such salen systems can also tune the Cu^{II}/Cu^I reduction potential.[41c]

3.4. Electronic Spectroscopy. *3.4.1. Chemical Oxidation of Ni(Sal^{CF3}).* The electronic absorption spectrum of **Ni(Sal^{CF3})** is typical of low-spin d^8 square-planar Ni^{II} bis-phenolate salen complexes (Figure 3).[12c,q] While no absorption was observed at energies lower than 20 000 cm^{-1} for the neutral form, two intense NIR transitions were observed upon oxidation. These sharp and intense NIR bands for $[\mathbf{Ni(Sal^{CF3})}]^{+\bullet}$ are observed at energies similar to those of $[\mathbf{Ni(Sal^{tBu})}]^{+\bullet}$ (^{t}Bu: $\nu = 4700$ cm^{-1}, $\varepsilon = 21\,600$ M^{-1} cm^{-1}, $\nu = 9100$ cm^{-1}, $\varepsilon = 7200$ M^{-1} cm^{-1}; CF$_3$: $\nu = 4900$ cm^{-1}, $\varepsilon = 16\,200$ M^{-1} cm^{-1}, $\nu = 8600$ cm^{-1}, $\varepsilon = 13\,100$ M^{-1} cm^{-1}). Indeed, the band shapes for both $[\mathbf{Ni(Sal^{tBu})}]^{+\bullet}$ and $[\mathbf{Ni(Sal^{CF3})}]^{+\bullet}$ are quite similar, suggesting that both oxidized species are Class III delocalized systems by the Robin−Day classification.[42] While the stability of the oxidized species precluded its isolation for further crystallo-

Table 2. Redox Potentials of Ni(Sal^R) Versus Fc$^+$/Fc^a

compound	$E_{1/2}^1$ (V)	$E_{1/2}^2$ (V)	ΔE_{ox} ($E_{1/2}^2 - E_{1/2}^1$) (V)	K_c
Ni(Sal^{NMe2})^b	−0.24 (0.14)	−0.08 (0.14)	0.16	2.9×10^3
Ni(Sal^{OMe})^b	0.22 (0.14)	0.59 (0.14)	0.37	1.0×10^8
Ni(Sal^{tBu})^b	0.37 (0.14)	0.85 (0.14)	0.48	2.4×10^{10}
Ni(Sal^{CF3})^c	0.78 (0.13)	1.19 (0.17)	0.38^b	1.7×10^8

^{a}Peak-to-peak differences in brackets ($|E_{pa} - E_{pc}|$ in V). Peak-to-peak difference for the Fc$^+$/Fc couple at 233 K is ca. 0.13 V, while at 298 K it is ca. 0.12 V. ^{b}CV performed at 233 K, ref 12c. ^{c}CV performed at 298 K.

Table 3. Redox Potentials of Cu(Sal^R) Complexes Versus Fc$^+$/Fc^a

compound	$E_{1/2}^1$ (V)	$E_{1/2}^2$ (V)
Cu(Sal^{OMe})^b	0.28	0.44
Cu(Sal^{tBu})^c	0.45	0.65
Cu(Sal^{CF3})^d	0.74 (0.16)	1.28 (0.16)

^{a}Peak-to-peak differences in brackets ($|E_{pa} - E_{pc}|$ in V). Peak-to-peak difference for the Fc$^+$/Fc couple at 233 K is ca. 0.13 V, while at 298 K it is ca. 0.12 V. ^{b}CV performed at 233 K, ref 12q. ^{c}CV performed at 233 K, ref 37. ^{d}CV performed at 298 K.
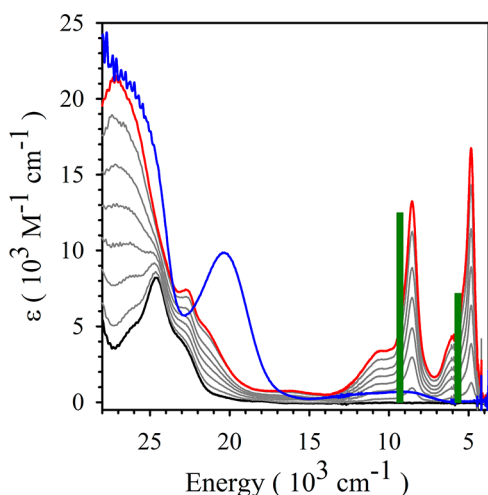

Figure 3. Electronic spectra of Ni(Sal^{CF3}) (black), [Ni(Sal^{CF3})]$^{+\bullet}$ (red), and [Ni^{III}(Sal^{CF3})(py)$_2$]$^+$ (blue). Intermediate gray lines measured during the oxidation titration with N(C$_6$H$_3$Br$_2$)$_3$SbF$_6$ in CH$_2$Cl$_2$ at 198 K. Green bars represent transitions predicted by TD-DFT.

graphic characterization ($t_{1/2}$ (298 K) ca. 80 min), the delocalized electronic structure is supported by EPR data and density functional theory (DFT) calculations (vide infra). Interestingly, while [Ni(Sal^{tBu})]$^{+\bullet}$ and [Ni(Sal^{CF3})]$^{+\bullet}$ both exhibit delocalized electronic structures, the relative intensity of their respective NIR features differ, and this is further explored by TD-DFT calculations (vide infra).

3.4.2. Pyridine Binding to [Ni(Sal^{CF3})]$^{+\bullet}$. The addition of 30 equiv of pyridine to [Ni(Sal^{CF3})]$^{+\bullet}$ in solution results in the loss of the NIR transitions and emergence of a new transition at 20 300 cm^{-1} (Blue spectrum, Figure 3). This spectral pattern has been previously observed for the axial binding of two pyridines to [Ni(Sal^{tBu})]$^{+\bullet}$ to form [Ni^{III}(Sal^{tBu})(py)$_2$]$^+$, with an accompanying shift in the locus of oxidation from the ligand to metal.[12g] Binding affinities of pyridine to [Ni(Sal^R)]$^{+\bullet}$ (R = ^{t}Bu, CF$_3$) were determined by incremental addition of pyridine to a solution of the oxidized species (Supporting Information,

Figures S3 and S4), and the resultant data were fit according to eq 4.

$$\log \beta_2 = \frac{[[\text{Ni}^{III}(\text{Sal}^R)(\text{py})_2]^+]}{[[\text{Ni}(\text{Sal}^R)]^{+\bullet}][\text{py}]^2} \tag{4}$$

At 198 K, [Ni(Sal^{tBu})]$^{+\bullet}$ and [Ni(Sal^{CF3})]$^{+\bullet}$ exhibited log β_2 values of 7.7 ± 0.2 M^{-2} and 12.4 ± 1.1 M^{-2}, respectively. The higher binding constant for [Ni(Sal^{CF3})]$^{+\bullet}$ reflects the expected increase in electrophilicity of the Ni center chelated by an electron poor ligand. The formation of [Ni(Sal^{CF3})]$^{+\bullet}$ and [Ni^{III}(Sal^{CF3})(py)$_2$]$^+$ is further evidenced by EPR spectroscopy (vide infra).

3.4.3. Chemical Oxidation of Cu(Sal^{CF3}). The electronic absorption spectrum of Cu(Sal^{CF3}) is typical of low-spin d^9 square-planar Cu^{II} bis(phenolate) salen complexes, with an intense charge transfer transition at 28 000 cm^{-1} (ε = 12 500 M^{-1} cm^{-1}) and a weak d−d transition at 17 600 cm^{-1} (ε = 600 M^{-1} cm^{-1}; Figure 4).[12f,q] The oxidation of Cu(Sal^{CF3}) leads to
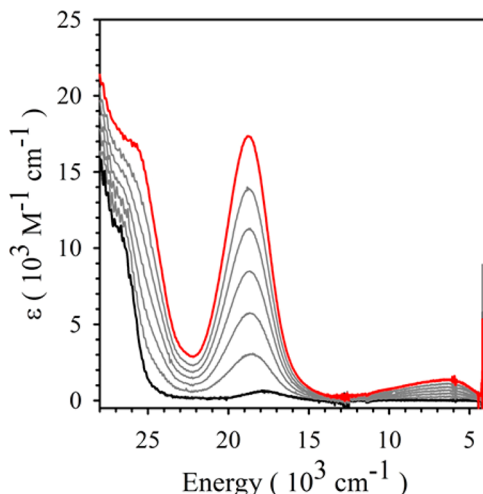

Figure 4. Electronic spectra of Cu(Sal^{CF3}) (black) and [Cu(Sal^{CF3})]$^+$ (red) in CH$_2$Cl$_2$ at 198 K. Intermediate gray lines measured during the oxidation titration with N(C$_6$H$_3$Br$_2$)$_3$SbF$_6$.

the appearance of two new bands at 18 700 cm^{-1} (ε = 17 300 M^{-1} cm^{-1}) and 6300 cm^{-1} (ε = 1400 M^{-1} cm^{-1}), which are in line with a previous report.[12f] The emergence of the intense band at ca. 18 000 cm^{-1} has been linked to the formation of a Cu^{III} species (LMCT transition), as observed for [Cu(Sal^{tBu})]$^+$ at low temperature (ε = 14 000 M^{-1} cm^{-1}).[12f] In comparison, no such band was observed for [Cu(Sal^{OMe})]$^+$, in which the formation of a Cu^{II}-phenoxyl radical species is favored due to the electron-donating ability of the *para*-OMe moiety.[12q] In addition, the intensity of the band at ca. 18 000 cm^{-1} for [Cu(Sal^{tBu})]$^+$ is reduced by 50% upon warming from 198 to 298 K, signifying a reversible temperature-dependent equili-

brium between a Cu^{III} species at low temperature and a Cu^{II}-phenoxyl radical species at room temperature.[12f] This effect could not be probed for $[\mathbf{Cu(Sal^{CF3})}]^+$ above 233 K due to the thermal instability at 273 K, as evident by the irreversible decrease in the LMCT transition with warming (Supporting Information, Figure S5).

3.5. Continuous Wave X-band Electron Paramagnetic Resonance. The X-band EPR spectrum of $[\mathbf{Ni(Sal^{CF3})}]^{+\bullet}$ collected at 195 K in CH_2Cl_2 showed a broad isotropic signal at $g_{iso} = 2.067$ (Figure 5a and Table 4). A minor signal at $g = 2.003$
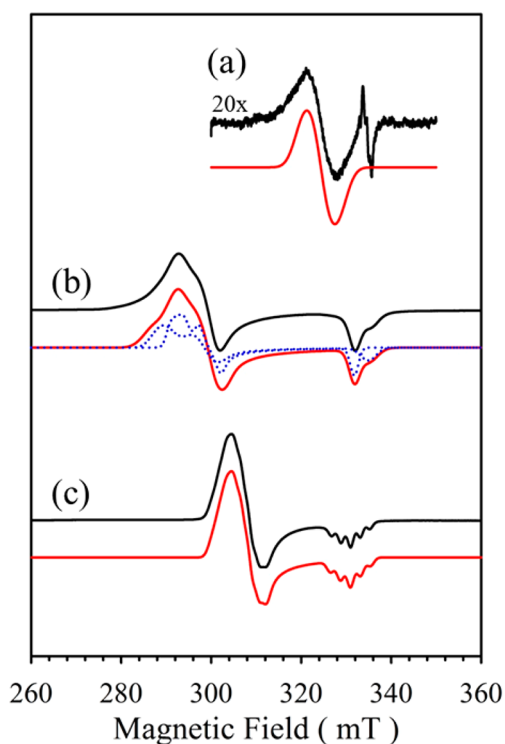

Figure 5. X-band EPR spectra for: (a) $[\mathbf{Ni(Sal^{CF3})}]^{+\bullet}$ at 195 K; (b) $[\mathbf{Ni^{III}(Sal^{CF3})(D)_x}]^+$ (x = 1 or 2) at 20 K and (c) $[\mathbf{Ni^{III}(Sal^{CF3})(py)_2}]^+$ at 20 K in CH_2Cl_2. Experimental spectrum: black. Overall simulations: red. Individual species: blue dotted. Conditions: Frequency: (a) 9.386 GHz, (b) 9.383 GHz, and (c) 9.380 GHz; Power: 2.0 mW; modulation frequency: 100 kHz; amplitude 0.6 mT. See Experimental Section for details.

Table 4. X-Band EPR Simulation Parameters for $[\mathbf{Ni(Sal^{CF3})}]^{+\bullet}$ Complexes

compound[a]	g_x	g_y	g_z	g_{av}
$[\mathbf{Ni(Sal^{CF3})}]^{+\bullet}$, 195 K[b]				2.067
$[\mathbf{Ni(Sal^{CF3})}]^{+\bullet}$, 20 K, S_1[c]	2.328	2.247	2.001	2.192
$[\mathbf{Ni(Sal^{CF3})}]^{+\bullet}$, 20 K, S_2[c]	2.291	2.234	2.020	2.182
$[\mathbf{Ni^{III}(Sal^{CF3})(py)_2}]^+$, 20 K[c]	2.209	2.171	2.025	2.135

[a]S_1 = species 1; S_2 = species 2. [b]Collected in a capillary tube. [c]Collected in a 4 mm outer diameter EPR tube.

is preliminarily assigned as an organic decomposition product, accounting for 3% of the overall signal by spin integration. Because of solvent effects, collection of this spectrum was performed in a capillary tube with a much smaller sample volume, resulting in decreased signal strength. The observed g-value suggests increased metal contribution to the SOMO when compared to other $[\mathbf{Ni(Sal^R)}]^{+\bullet}$ complexes,[12c] which is further corroborated with DFT calculations (vide infra). When

the sample was frozen, a rhombic spectrum consisting of two components with g_{av} of ca. 2.18 was observed (20 K), indicating the formation of two distinct Ni^{III} species (Figure 5b). This likely arises from the axial ligation of a donor species (D, most likely adventitious H_2O from sample preparation) in solution upon freezing, as the g_{av} suggests a shift in the locus of oxidation from ligand to metal to generate a $[\mathbf{Ni^{III}(Sal^{CF3})}^-(\mathbf{D})_x]^+$ (x = 1 or 2) species. In contrast, the EPR spectrum of $[\mathbf{Ni(Sal^{tBu})}]^{+\bullet}$ at 20 K, prepared under the same conditions, exhibits a ligand radical g-value (g_1 = 2.063, g_2 = 2.013, g_3 = 1.988, g_{av} = 2.021), indicating that $[\mathbf{Ni(Sal^{tBu})}]^{+\bullet}$ maintains ligand radical character upon freezing.[38] As expected, the addition of 30 equiv of pyridine and subsequent freezing results in a rhombic spectrum, which was observed previously in the formation of $[\mathbf{Ni^{III}(Sal^{tBu})(py)_2}]^+$ (Figure 5c).[12g] In addition, hyperfine coupling to the two nitrogen nuclei from the pyridine moieties was observed. The shift in g-value between frozen $[\mathbf{Ni(Sal^{CF3})}]^{+\bullet}$ and $[\mathbf{Ni^{III}(Sal^{CF3})(py)_2}]^+$ suggests that it is sensitive to the identity of the axial ligand. This was observed previously for a DMF adduct of $[\mathbf{Ni(Sal^{tBu})}]^{+\bullet}$.[12n]

The X-band EPR spectrum of $\mathbf{Cu(Sal^{CF3})}$ collected at 20 K exhibited features consistent with a square-planar d^9 Cu^{II} center as observed for other $\mathbf{Cu(Sal^R)}$ complexes (Figure 6, simulation

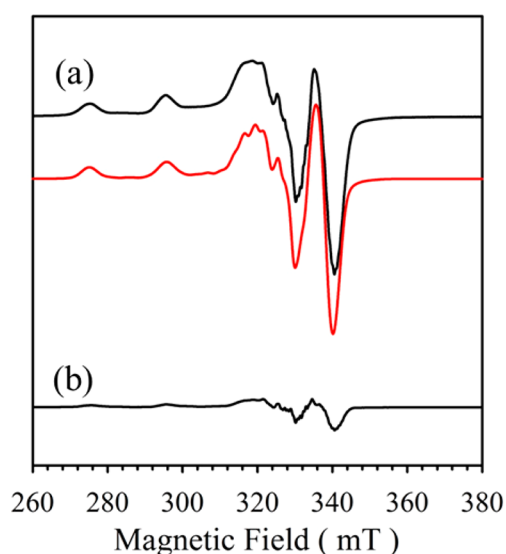**Figure 6.** X-band EPR spectra for concentration matched samples of: (a) $\mathbf{Cu(Sal^{CF3})}$ and (b) $[\mathbf{Cu(Sal^{CF3})}]^+$ in CH_2Cl_2 at 20 K. Experimental spectrum: black. Simulation: red. Conditions: Frequency: (a) 9.383 GHz and (b) 9.382 GHz; Power: 2.0 mW; modulation frequency: 100 kHz; amplitude 0.6 mT.

parameters: $g_{\parallel}$ = 2.193, $g_{\perp}$ = 2.046, $A_{Cu\parallel}$ = 575, $A_{N\parallel}$ = 85, $A_{Cu\perp}$ = 30, $A_{N\perp}$ = 40, A values in MHz).[12q,37] Oxidation of $\mathbf{Cu(Sal^{CF3})}$ to $[\mathbf{Cu(Sal^{CF3})}]^+$ results in a substantial decrease in the EPR signal to <10% of the original intensity by spin integration, which supports the formation of a Cu^{III} species as suggested by the UV−vis experiment. The weak EPR signal of $[\mathbf{Cu(Sal^{CF3})}]^+$ may arise from its thermal decomposition during sample preparation or from remaining unoxidized $\mathbf{Cu(Sal^{CF3})}$.

3.6. ^{19}F Nuclear Magnetic Resonance. Complementing the electrochemical measurements, UV−vis−NIR spectra, and EPR data, ^{19}F NMR was used as an additional tool for evaluating the electronic structure of $\mathbf{Ni(Sal^{CF3})}$, $\mathbf{Cu(Sal^{CF3})}$, and the one-electron oxidized forms. Referenced to $CFCl_3$, sharp peaks were observed for the ligands $\mathbf{H_2(Sal^{CF3})}$ and

Ni(Sal^{CF3}) at −62.8 ppm and −62.5 ppm, respectively (Figure 7a,b, Supporting Information, Figure S6, Table 5). These
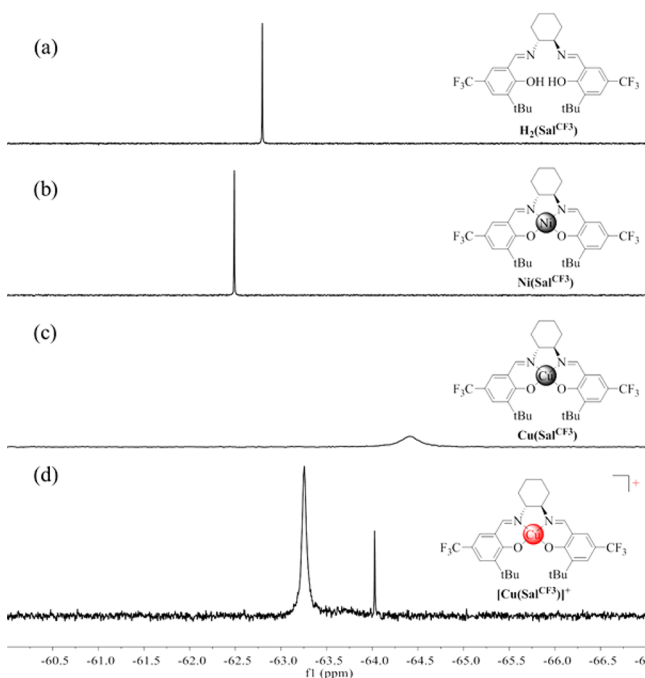

Figure 7. ^{19}F NMR spectra of (a) **H$_2$(Sal^{CF3})**, (b) **Ni(Sal^{CF3})**, (c) **Cu(Sal^{CF3})**, and (d) **[Cu(Sal^{CF3})]$^+$** recorded in CH$_2$Cl$_2$ at 298 K.

Table 5. ^{19}F NMR Chemical Shifts

compound	chemical Shift (ppm)^a	$W_{1/2}$ (Hz)
H$_2$(Sal^{CF3})	−62.8	3
Ni(Sal^{CF3})	−62.5	3
[Ni(Sal^{CF3})]$^{+\bullet}$		
Cu(Sal^{CF3})	−64.4	135
[Cu(Sal^{CF3})]$^+$	−63.2	35
	−64.0	3

^{a}Chemical shift relative to CFCl$_3$.

chemical shifts are in agreement with other diamagnetic phenol-containing compounds bearing a CF$_3$ moiety.[22,43] Peak widths at half height ($W_{1/2}$) for both **H$_2$(Sal^{CF3})** and **Ni(Sal^{CF3})** were 3 Hz, as expected for a diamagnetic compound (Table 5). On the other hand, **Cu(Sal^{CF3})** exhibited a broad signal at −64.4 ppm with $W_{1/2}$ = 135 Hz due to the paramagnetic Cu^{II} center (Figure 7c). The ^{19}F peak for **Ni(Sal^{CF3})** disappears upon oxidation to **[Ni(Sal^{CF3})]$^{+\bullet}$**, consistent with the formation of a ligand radical in close proximity to the CF$_3$ moieties (Supporting Information, Figure S7). In contrast, loss of the broad ^{19}F signal of **Cu(Sal^{CF3})** was accompanied by the appearance of two signals upon oxidation to **[Cu(Sal^{CF3})]$^+$** (Figure 7d), namely, a major signal at −63.2 ppm ($W_{1/2}$ = 35 Hz) and a minor signal at −64.0 ppm ($W_{1/2}$ = 3 Hz). The minor signal is attributed to a decomposition product from the oxidation reaction and increases over time (Table 5, Supporting Information, Figure S9).

The decomposition is consistent with the limited stability of **[Cu(Sal^{CF3})]$^+$** in solution ($t_{1/2}$ = 150 min at 298 K). The relatively sharp ^{19}F peak for **[Cu(Sal^{CF3})]$^+$** is assigned to a Cu^{III} species (Figure 7d); the broadness in the signal is likely due to fast electron exchange with a paramagnetic decomposition

product. Note that the signal for the SbF$_6^-$ counterion could not be detected due to the quadrupolar moment of the Sb center.[44]

3.7. X-ray Photoelectron Spectroscopy. Ni and Cu XPS was used to evaluate the metal oxidation states in both the neutral and oxidized complexes in the solid state. Referenced to the C 1s binding energy, the metal 2p$_{3/2}$ and 2p$_{1/2}$ binding energies (Table 6) for both neutral complexes indicate a

Table 6. Metal (2p) Binding Energies Versus C(1s) (284.8 eV)

compound	binding energy (eV)	
	2p$_{3/2}$	2p$_{1/2}$
Ni(Sal^{CF3})	872.1	854.8
[Ni(Sal^{CF3})]$^{+\bullet}$	872.1	854.9
Cu(Sal^{CF3})	954.0	934.1
[Cu(Sal^{CF3})]$^+$	955.9	935.9

common 2+ oxidation state, as previously observed for structurally similar Ni[45] and Cu[12f] complexes. Upon oxidation, the Ni 2p$_{3/2}$ and 2p$_{1/2}$ binding energies for **[Ni(Sal^{CF3})]$^{+\bullet}$** experience a small shift toward higher energies (Supporting Information, Figure S10 and Table 6), supporting the formation of a Ni^{II}-phenoxyl rather than a Ni^{III}-phenolate species in the solid state. Fluorine KLL peaks (Auger transition) at 856.8 and 876.2 eV are also visible in both the oxidized Ni and Cu complexes (Supporting Information, Figure S11).[46] However, a larger shift in binding energy (ca. 1.8 eV, Supporting Information, Figure S12) was observed from oxidation of **Cu(Sal^{CF3})** to **[Cu(Sal^{CF3})]$^+$**. This indicates a change in Cu oxidation state from 2+ to 3+, consistent with a previous report on **[Cu(Sal^{tBu})]$^+$**, which showed a shift in binding energy of ca. 1.8 eV in comparison to its neutral form.

3.8. Theoretical Analysis. *3.8.1. Ni(Sal^{CF3}).* A symmetric structure was predicted for **Ni(Sal^{CF3})** using the B3LYP functional with a PCM for CH$_2$Cl$_2$ (Supporting Information, Table S1). A symmetric structure was also predicted for **[Ni(Sal^{CF3})]$^{+\bullet}$**, with a contraction in the coordination sphere in comparison to **Ni(Sal^{CF3})** (Table S1). A delocalized electronic structure, in which the ligand radical is distributed over both aromatic phenolates, was predicted for **[Ni(Sal^{CF3})]$^{+\bullet}$** (Figure 8), in agreement with the sharp and intense NIR bands observed in the UV−vis−NIR spectrum (Figure 3). The predicted spin density on the nickel center for **[Ni(Sal^{CF3})]$^{+\bullet}$** (SD$_{Ni}$: 34%), and thus metal contribution to the SOMO, is higher in comparison to other **[Ni(Sal^R)]$^{+\bullet}$** complexes (**[Ni(Sal^{tBu})]$^{+\bullet}$**: SD$_{Ni}$: 22%; **[Ni(Sal^{OMe})]$^{+\bullet}$**: SD$_{Ni}$: 12%; **[Ni(Sal^{NMe2})]$^{+\bullet}$**: SD$_{Ni}$: 5%). This observation follows the
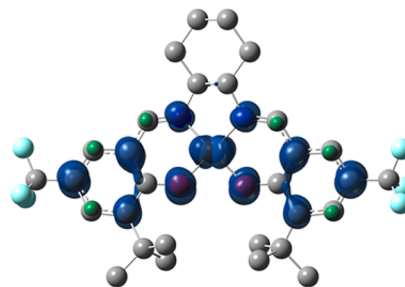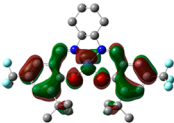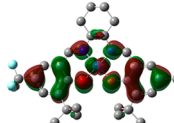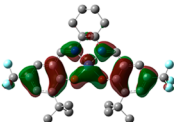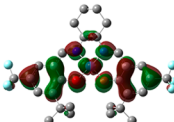
Figure 8. Spin density plot of **[Ni(Sal^{CF3})]$^{+\bullet}$** (SD$_{Ni}$ = 34%). See Experimental Section for calculation details.

trends established previously for other $[\mathbf{Ni(Sal^R)}]^{+\bullet}$ complexes, where electron-donating *para*-ring substituents decrease the metal contribution to the SOMO,[12c,47] and is in agreement with the increased *g*-value in the EPR spectrum of $[\mathbf{Ni(Sal^{CF3})}]^{+\bullet}$ (Figure 5). Using CAM-B3LYP as the functional with no solvent model also predicted a symmetric structure for $[\mathbf{Ni(Sal^{CF3})}]^{+\bullet}$, albeit with slightly different SD_{Ni} values.[47]

TD-DFT calculations[33] were undertaken to gain insight into the spectral features of $[\mathbf{Ni(Sal^{CF3})}]^{+\bullet}$. Two NIR transitions were predicted for $[\mathbf{Ni(Sal^{CF3})}]^{+\bullet}$ (Figure 3), and the natural transition orbitals (NTOs)[48] contributing to the transitions are shown in Table 7.

Table 7. Natural Transition Orbitals Representing the Transitions Contributing to the Two NIR Bands[a] of $[\mathbf{Ni(Sal^{CF3})}]^{+\bullet}$

Excited State Properties	Holes	Electrons
Excited State 1 ν_{calc} = 5700 cm^{-1} f = 0.0717 ν_{exp} = 4900 cm^{-1} ε = 16200 M^{-1} cm^{-1}		
Excited State 3 ν_{calc} = 9300 cm^{-1} f = 0.1248 ν_{exp} = 8600 cm^{-1} ε = 13100 M^{-1} cm^{-1}		

[a]See Experimental Section for calculation details.

The lowest energy transition predicted at 5700 cm^{-1} matches well with the experimental energy and is predicted to be a delocalized intraligand charge transfer (ILCT) transition, with donation to the imine nitrogens. The higher energy band (9300 cm^{-1}) is predicted to be more intense, and the NTOs involved are fully delocalized over the ligand framework (Table 7). Such intense NIR transitions have also been predicted for the similarly delocalized species $[\mathbf{Ni(Sal^{tBu})}]^{+\bullet}$ (Supporting Information, Table S2).[12c] These calculations support the experimental data obtained in these studies in the assignment of $[\mathbf{Ni(Sal^{CF3})}]^{+\bullet}$ as a Class III intervalence compound.

3.8.2. Cu(Sal^{CF3}). A symmetric structure was predicted for $\mathbf{Cu(Sal^{CF3})}$ within ±0.01 Å of the experimental values using the B3LYP functional with a PCM for CH_2Cl_2 (Table S1). The predicted spin density of $\mathbf{Cu(Sal^{CF3})}$ shows spin-covalency between the Cu $d_{x^2-y^2}$ orbital and the coordinating atoms, as expected for a d^9 metal complex (Supporting Information, Figure S12).

Oxidation of $\mathbf{Cu(Sal^{CF3})}$ can afford one of three electronic states: (i) a d^8 Cu^{III}-salen complex (S = 0), (ii) a Cu^{II} complex antiferromagnetically coupled to a phenoxyl radical (broken symmetry, S = 0), or (iii) a Cu^{II} complex ferromagnetically coupled to a phenoxyl radical (S = 1). All three possibilities were explored, where the broken symmetry solution converges to the singlet solution, which has been observed previously for calculations of $[\mathbf{Cu(Sal^{tBu})}]^+$ using the same level of theory.[12f]

The S = 0 solution for $[\mathbf{Cu(Sal^{CF3})}]^+$ was predicted to be lowest in energy by 3.3 kcal/mol, which is in agreement with the experimental data. This is consistent with $[\mathbf{Cu(Sal^{CF3})}]^+$ being a Cu^{III}-salen species, in comparison to $[\mathbf{Cu(Sal^{tBu})}]^+$ where an equilibrium between Cu^{III}-salen and a Cu^{II}-phenoxyl radical species was observed.

4. DISCUSSION AND SUMMARY

Chemical oxidation of $\mathbf{Ni(Sal^{CF3})}$ monitored by UV–vis–NIR showed the formation of a delocalized ligand-radical species, evidenced by the appearance of sharp and intense NIR transitions (Figure 3). This is supported by a negligible shift in metal binding energy by XPS as well as the disappearance of the ^{19}F NMR signal upon oxidation. An isotropic signal (g = 2.067) indicative of a ligand radical was observed in the solution-state EPR of $[\mathbf{Ni(Sal^{CF3})}]^{+\bullet}$, and this *g*-value is higher in comparison to those of other $[\mathbf{Ni(Sal^R)}]^{+\bullet}$, consistent with an increase in metal character for the SOMO of $[\mathbf{Ni(Sal^{CF3})}]^{+\bullet}$ due to the electron-withdrawing CF$_3$ substituents (Figure 5a). Interestingly, a rhombic signal comprised of two species at $g_{av} \approx$ 2.18 was observed when the sample was frozen, signifying the formation of a Ni^{III} species (Figure 5b). Typically, a low-spin S = 1/2 Ni^{III} center will display such a rhombic EPR pattern with g_{av} values ca. 2.12–2.17.[16,18,49] The EPR spectrum of $[\mathbf{Ni(Sal^{CF3})}]^{+\bullet}$ exhibits two similar $g_{\parallel}$ (g_x and g_y) and $g_{\perp}$ (g_z) features, a pattern that is consistent with previous reports of five- or six-coordinate Ni^{III} species.[16,18,49,50] This is in contrast to four-coordinate Ni^{III} species, where a single $g_{\parallel}$ and two similar $g_{\perp}$ components are observed.[16] This suggests the shift in oxidation locus of $[\mathbf{Ni(Sal^{CF3})}]^{+\bullet}$ upon freezing is due to adventitious axial ligand binding, a process that is favored in comparison to $[\mathbf{Ni(Sal^{tBu})}]^{+\bullet}$, as a result of increased Lewis acidity of the Ni center.

TD-DFT calculations further support a delocalized electronic structure, correctly predicting the two intense NIR electronic transitions for $[\mathbf{Ni(Sal^{CF3})}]^{+\bullet}$. Interestingly, the two low-energy bands display a similar intensity (Figure 3), while for $[\mathbf{Ni(Sal^{tBu})}]^{+\bullet}$ (Supporting Information, Figure S15) the lowest energy transition is threefold more intense. To gain further insight into this difference we analyzed the TD-DFT transitions employing NTOs.[48] While the calculated oscillator strengths do not correctly predict the experimental ratio observed for $[\mathbf{Ni(Sal^{CF3})}]^{+\bullet}$, the change in predicted band intensities in comparison to $[\mathbf{Ni(Sal^{tBu})}]^{+\bullet}$ (Supporting Information, Figure S15) offers insight into the nature of the electronic transitions for these two ligand radical complexes. For $[\mathbf{Ni(Sal^{CF3})}]^{+\bullet}$, the low-energy transition is predicted to have significant ILCT character with donation to the imine nitrogens (Table 7), while the NTOs for the higher energy transition are fully delocalized, and the increased intensity reflects greater overlap between the donor and acceptor orbitals.[51] For $[\mathbf{Ni(Sal^{tBu})}]^{+\bullet}$, the higher energy transition is predicted to have significant donation to the phenolate oxygens (Table S2), while the NTOs for the lowest energy transition are fully delocalized with significant overlap between the donor and acceptor orbitals. These data suggest that the *para*-ring electron-withdrawing group not only serves to increase the charge density on the Ni center but also alters the nature of the low-energy ligand-radical electronic transitions.

Upon oxidation, $[\mathbf{Cu(Sal^{CF3})}]^+$ demonstrates the characteristics of a diamagnetic species, with a significant decrease in the EPR signal (Figure 6) as well as the sharpening of the ^{19}F NMR signal (Figure 7). This was further evidenced by the appearance

of an intense transition at ca. 18 000 $M^{-1}cm^{-1}$ in the UV−vis−NIR spectra, a characteristic LMCT for a Cu^{III}-salen complex, suggesting the locus of oxidation for $[Cu(Sal^{CF3})]^+$ is primarily metal-based. XPS measurements further support $[Cu(Sal^{CF3})]^+$ as a Cu^{III} species in the solid state, where the binding energy of the metal center is shifted upwards of 1.8 eV upon oxidation from its neutral counterpart. Interestingly, $[Cu(Sal^{tBu})]^+$ exists in a reversible temperature-dependent equilibrium in solution between a Cu^{III}-phenolate and a Cu^{II}-phenoxyl species, which is manifested in a reduction of its LMCT band by ca. 50% upon an increase in temperature.[12f] This equilibrium could not be probed fully for $[Cu(Sal^{CF3})]^+$ due to its thermal instability above 233 K ($t_{1/2}$ = 150 min at 298 K, Supporting Information, Figure S5). However, spectra at 198 and 233 K do not show appreciable differences (Supporting Information, Figure S5), suggesting that in this temperature range the Cu^{III}-phenolate electronic state is stabilized. The significant decrease in the electronic spectra at 273 K is attributed to decomposition. In addition, the calculated electronic energies support the formation of a Cu^{III}-phenolate species, where this electronic state is favored over a triplet Cu^{II}-phenoxyl radical species by 3.3 kcal/mol. Under the same calculation parameters, the $S = 1$ Cu^{II}-phenoxyl radical solution for $[Cu(Sal^{tBu})]^+$ is favored by 1.3 kcal/mol,[12f] further supporting that $[Cu(Sal^{CF3})]^+$ exhibits greater Cu^{III} character in comparison to $[Cu(Sal^{tBu})]^+$. Overall, these results show that Ni and Cu complexes of the electron-poor salen ligand H_2Sal^{CF3} afford a delocalized phenoxyl radical complex for Ni and a high-valent metal complex in the case of Cu.

ASSOCIATED CONTENT

Ⓢ Supporting Information

Full citation for reference 28, cif file of $Cu(Sal^{CF3})$, Hammett analysis of oxidative potentials of $Ni(Sal^R)$, pyridine binding titrations for $Ni(Sal^{CF3})$, variable-temperature UV−vis−NIR spectra of $[Cu(Sal^{CF3})]^+$, XPS spectra, additional ^{19}F NMR plots, experimental and calculated coordination sphere metrical parameters, calculated natural transition orbitals, calculated spin density plot, calculated optimized coordinates, TD-DFT excitation energies and oscillator strengths. The Supporting Information is available free of charge on the ACS Publications website at DOI: 10.1021/acs.inorgchem.5b00783.

AUTHOR INFORMATION

Corresponding Author

*E-mail: tim_storr@sfu.ca.

Notes

The authors declare no competing financial interest.

ACKNOWLEDGMENTS

REFERENCES

(1) (a) Lyons, C. T.; Stack, T. D. P. *Coord. Chem. Rev.* **2013**, *257*, 528−540. (b) Luca, O. R.; Crabtree, R. H. *Chem. Soc. Rev.* **2013**, *42*, 1440−1459. (c) de Bruin, B. *Eur. J. Inorg. Chem.* **2012**, 340−342. (d) Lyaskovskyy, V.; de Bruin, B. *ACS Catal.* **2012**, *2*, 270−279. (e) Kaim, W. *Eur. J. Inorg. Chem.* **2012**, 343−348. (f) Chirik, P. J. *Inorg. Chem.* **2011**, *50*, 9737−9740.

(2) (a) Whittaker, J. W. *Chem. Rev.* **2003**, *103*, 2347−2363. (b) Thomas, F.; et al. *Stable Radicals: Fundamentals and Applied Aspects of Odd-Electron Compounds*; Hicks, R., Ed.; Wiley: Hoboken, NJ, 2010; pp 1−588.

(3) Rittle, J.; Green, M. T. *Science* **2010**, *330*, 933−937.

(4) (a) Hendrickson, D. N.; Pierpont, C. G. Valence Tautomeric Transition Metal Complexes. In *Spin Crossover in Transition Metal Compounds II*; Springer: New York, 2004; Vol. 234, pp 63−95. (b) Pierpont, C. G. *Coord. Chem. Rev.* **2001**, *219*, 415−433. (c) Pierpont, C. G. *Coord. Chem. Rev.* **2001**, *216*, 99−125. (d) Pierpont, C. G.; Lange, C. W. The Chemistry of Transition-Metal Complexes Containing Catechol and Semiquinone Ligands. In *Progress in Inorganic Chemistry*; Karlin, K. D., Ed.; Wiley: Hoboken, NJ, **1994**; Vol. *41*, pp 331−442.

(5) (a) Ray, K.; George, S. D.; Solomon, E. I.; Wieghardt, K.; Neese, F. *Chem.—Eur. J.* **2007**, *13*, 2783−2797. (b) Ray, K.; Weyhermuller, T.; Neese, F.; Wieghardt, K. *Inorg. Chem.* **2005**, *44*, 5345−5360.

(6) (a) Chaudhuri, P.; Wieghardt, K. Phenoxyl Radical Complexes. In *Progress in Inorganic Chemistry*; Wiley: Hoboken, NJ, **2001**; Vol. 50, pp 151−216. (b) Allard, M. M.; Sonk, J. A.; Heeg, M. J.; McGarvey, B. R.; Schlegel, H. B.; Verani, C. N. *Angew. Chem., Int. Ed.* **2012**, *51*, 3178−3182.

(7) (a) Bachler, V.; Olbrich, G.; Neese, F.; Wieghardt, K. *Inorg. Chem.* **2002**, *41*, 4179−4193. (b) Herebian, D.; Bothe, E.; Bill, E.; Weyhermuller, T.; Wieghardt, K. *J. Am. Chem. Soc.* **2001**, *123*, 10012−10023. (c) Mederos, A.; Dominguez, S.; Hernandez-Molina, R.; Sanchiz, J.; Brito, F. *Coord. Chem. Rev.* **1999**, 193-5, 857−911. (d) Peng, S. M.; Chen, C. T.; Liaw, D. S.; Chen, C. I.; Yu, W. *Inorg. Chim. Acta* **1985**, *101*, L31−L33.

(8) (a) Bill, E.; Bothe, E.; Chaudhuri, P.; Chlopek, K.; Herebian, D.; Kokatam, S.; Ray, K.; Weyhermuller, T.; Neese, F.; Wieghardt, K. *Chem.—Eur. J.* **2004**, *11*, 204−224. (b) Blackmore, K. J.; Sly, M. B.; Haneline, M. R.; Ziller, J. W.; Heyduk, A. F. *Inorg. Chem.* **2008**, *47*, 10522−10532. (c) Smith, A. L.; Hardcastle, K. I.; Soper, J. D. *J. Am. Chem. Soc.* **2010**, *132*, 14358−14360. (d) Rajput, A.; Sharma, A. K.; Barman, S. K.; Koley, D.; Steinert, M.; Mukherjee, R. *Inorg. Chem.* **2014**, *53*, 36−48. (e) Das, D.; Agarwala, H.; Chowdhury, A. D.; Patra, T.; Mobin, S. M.; Sarkar, B.; Kaim, W.; Lahiri, G. K. *Chem.—Eur. J.* **2013**, *19*, 7384−7394. (f) Das, D.; Scherer, T. M.; Das, A.; Mondal, T. K.; Mobin, S. M.; Fiedler, J.; Luis Priego, J.; Jimenez-Aparicio, R.; Kaim, W.; Lahiri, G. K. *Dalton Trans.* **2012**, *41*, 11675−11683. (g) Huebner, R.; Sarkar, B.; Fiedler, J.; Zalis, S.; Kaim, W. *Eur. J. Inorg. Chem.* **2012**, 3569−3576.

(9) (a) Bart, S. C.; Chlopek, K.; Bill, E.; Bouwkamp, M. W.; Lobkovsky, E.; Neese, F.; Wieghardt, K.; Chirik, P. J. *J. Am. Chem. Soc.* **2006**, *128*, 13901−13912. (b) Bowman, A. C.; Sproules, S.; Wieghardt, K. *Inorg. Chem.* **2012**, *51*, 3707−3717. (c) de Bruin, B.; Bill, E.; Bothe, E.; Weyhermuller, T.; Wieghardt, K. *Inorg. Chem.* **2000**, *39*, 2936−2947. (d) England, J.; Scarborough, C. C.; Weyhermuller, T.; Sproules, S.; Wieghardt, K. *Eur. J. Inorg. Chem.* **2012**, 4605−4621. (e) Lu, C. C.; Bill, E.; Weyhermuller, T.; Bothe, E.; Wieghardt, K. *J. Am. Chem. Soc.* **2008**, *130*, 3181−3197. (f) Lu, C. C.; George, S. D.; Weyhermuller, T.; Bill, E.; Bothe, E.; Wieghardt, K. *Angew. Chem., Int. Ed.* **2008**, *47*, 6384−6387. (g) Lu, C. C.; Weyhermuller, T.; Bill, E.; Wieghardt, K. *Inorg. Chem.* **2009**, *48*, 6055−6064. (h) Scarborough, C. C.; Sproules, S.; Weyhermuller, T.; DeBeer, S.; Wieghardt, K. *Inorg. Chem.* **2011**, *50*, 12446−12462. (i) Tondreau, A. M.; Milsmann, C.; Patrick, A. D.; Hoyt, H. M.; Lobkovsky, E.; Wieghardt, K.; Chirik, P. J. *J. Am. Chem. Soc.* **2010**, *132*, 15046−15059. (j) Wang, M.; England, J.; Weyhermuller, T.; Wieghardt, K. *Inorg. Chem.* **2014**, *53*, 2276−2287. (k) Wang, M.; Weyhermuller, T.; England, J.; Wieghardt, K. *Inorg. Chem.* **2013**, *52*, 12763−12776.

(10) (a) Adhikari, D.; Mossin, S.; Basuli, F.; Huffman, J. C.; Szilagyi, R. K.; Meyer, K.; Mindiola, D. J. *J. Am. Chem. Soc.* **2008**, *130*, 3676−3682. (b) Atienza, C. C. H.; Bowman, A. C.; Lobkovsky, E.; Chirik, P. J. *J. Am. Chem. Soc.* **2010**, *132*, 16343−16345. (c) Buttner, T.; Geier, J.; Frison, G.; Harmer, J.; Calle, C.; Schweiger, A.; Schonberg, H.; Grutzmacher, H. *Science* **2005**, *307*, 235−238. (d) Haneline, M. R.; Heyduk, A. F. *J. Am. Chem. Soc.* **2006**, *128*, 8410−8411.

(e) Koenigsmann, M.; Donati, N.; Stein, D.; Schoenberg, H.; Harmer, J.; Sreekanth, A.; Gruetzmacher, H. *Angew. Chem., Int. Ed.* **2007**, *46*, 3567−3570. (f) Maire, P.; Konigsmann, M.; Sreekanth, A.; Harmer, J.; Schweiger, A.; Grutzmacher, H. *J. Am. Chem. Soc.* **2006**, *128*, 6578−6580. (g) Miyazato, Y.; Wada, T.; Tanaka, K. *Bull. Chem. Soc. Jpn.* **2006**, *79*, 745−747. (h) Ringenberg, M. R.; Kokatam, S. L.; Heiden, Z. M.; Rauchfuss, T. B. *J. Am. Chem. Soc.* **2008**, *130*, 788−788. (i) Zarkesh, R. A.; Ziller, J. W.; Heyduk, A. F. *Angew. Chem., Int. Ed.* **2008**, *47*, 4715−4718.

(11) (a) Dolphin, D.; Niem, T.; Felton, R. H.; Fujita, I. *J. Am. Chem. Soc.* **1975**, *97*, 5288−5290. (b) Ohtsu, H.; Tanaka, K. *Angew. Chem., Int. Ed.* **2004**, *43*, 6301−6303. (c) Puschmann, F. F.; Harmer, J.; Stein, D.; Rueegger, H.; de Bruin, B.; Gruetzmacher, H. *Angew. Chem., Int. Ed.* **2010**, *49*, 385−389.

(12) (a) de Bellefeuille, D.; Askari, M. S.; Lassalle-Kaiser, B.; Journaux, Y.; Aukauloo, A.; Orio, M.; Thomas, F.; Ottenwaelder, X. *Inorg. Chem.* **2012**, *51*, 12796−12804. (b) Asami, K.; Tsukidate, K.; Iwatsuki, S.; Tani, F.; Karasawa, S.; Chiang, L.; Storr, T.; Thomas, F.; Shimazaki, Y. *Inorg. Chem.* **2012**, *51*, 12450−12461. (c) Chiang, L.; Kochem, A.; Jarjayes, O.; Dunn, T. J.; Vezin, H.; Sakaguchi, M.; Ogura, T.; Orio, M.; Shimazaki, Y.; Thomas, F.; Storr, T. *Chem.—Eur. J.* **2012**, *18*, 14117−14127. (d) Shimazaki, Y.; Arai, N.; Dunn, T. J.; Yajima, T.; Tani, F.; Ramogida, C. F.; Storr, T. *Dalton Trans.* **2011**, *40*, 2469−2479. (e) Shimazaki, Y.; Stack, T. D. P.; Storr, T. *Inorg. Chem.* **2009**, *48*, 8383−8392. (f) Storr, T.; Verma, P.; Pratt, R. C.; Wasinger, E. C.; Shimazaki, Y.; Stack, T. D. P. *J. Am. Chem. Soc.* **2008**, *130*, 15448−15459. (g) Storr, T.; Wasinger, E. C.; Pratt, R. C.; Stack, T. D. P. *Angew. Chem., Int. Ed.* **2007**, *46*, 5198−5201. (h) Rotthaus, O.; Jarjayes, O.; Del Valle, C. P.; Philouze, C.; Thomas, F. *Chem. Commun.* **2007**, 4462−4464. (i) Rotthaus, O.; Jarjayes, O.; Philouze, C.; Del Valle, C. P.; Thomas, F. *Dalton Trans.* **2009**, 1792−1800. (j) Rotthaus, O.; Jarjayes, O.; Thomas, F.; Philouze, C.; Del Valle, C. P.; Saint-Aman, E.; Pierre, J. L. *Chem.—Eur. J.* **2006**, *12*, 2293−2302. (k) Rotthaus, O.; Thomas, F.; Jarjayes, O.; Philouze, C.; Saint-Aman, E.; Pierre, J.-L. *Chem.—Eur. J.* **2006**, *12*, 6953−6962. (l) Kochem, A.; Jarjayes, O.; Baptiste, B.; Philouze, C.; Vezin, H.; Tsukidate, K.; Tani, F.; Orio, M.; Shimazaki, Y.; Thomas, F. *Chem.—Eur. J.* **2012**, *18*, 1068−1072. (m) Kochem, A.; Kanso, H.; Baptiste, B.; Arora, H.; Philouze, C.; Jarjayes, O.; Vezin, H.; Luneau, D.; Orio, M.; Thomas, F. *Inorg. Chem.* **2012**, *51*, 10557−10571. (n) Shimazaki, Y.; Tani, F.; Fukui, K.; Naruta, Y.; Yamauchi, O. *J. Am. Chem. Soc.* **2003**, *125*, 10512−10513. (o) Pratt, R. C.; Lyons, C. T.; Wasinger, E. C.; Stack, T. D. P. *J. Am. Chem. Soc.* **2012**, *134*, 7367−7377. (p) Verma, P.; Pratt, R. C.; Storr, T.; Wasinger, E. C.; Stack, T. D. P. *Proc. Natl. Acad. Sci. U.S.A.* **2011**, *108*, 18600−18605. (q) Orio, M.; Jarjayes, O.; Kanso, H.; Philouze, C.; Neese, F.; Thomas, F. *Angew. Chem., Int. Ed.* **2010**, *49*, 4989−4992. (r) Orio, M.; Philouze, C.; Jarjayes, O.; Neese, F.; Thomas, F. *Inorg. Chem.* **2010**, *49*, 646−658. (s) Kurahashi, T.; Fujii, H. *Inorg. Chem.* **2013**, *52*, 3908−3919. (t) Kurahashi, T.; Fujii, H. *Bull. Chem. Soc. Jpn.* **2012**, *85*, 940−947. (u) Kurahashi, T.; Fujii, H. *J. Am. Chem. Soc.* **2011**, *133*, 8307−8316. (v) Wang, C.; Kurahashi, T.; Fujii, H. *Angew. Chem., Int. Ed.* **2012**, *51*, 7809−7811.

(13) (a) Canali, L.; Sherrington, D. C. *Chem. Soc. Rev.* **1999**, *28*, 85−93. (b) Darensbourg, D. J. *Chem. Rev.* **2007**, *107*, 2388−2410. (c) Irie, R.; Noda, K.; Ito, Y.; Matsumoto, N.; Katsuki, T. *Tetrahedron Lett.* **1990**, *31*, 7345−7348. (d) Jacobsen, E. N.; Zhang, W.; Muci, A. R.; Ecker, J. R.; Deng, L. *J. Am. Chem. Soc.* **1991**, *113*, 7063−7064. (e) McGarrigle, E. M.; Gilheany, D. G. *Chem. Rev.* **2005**, *105*, 1563−1602.

(14) Dunn, T. J.; Chiang, L.; Ramogida, C. F.; Hazin, K.; Webb, M. I.; Katz, M. J.; Storr, T. *Chem.—Eur. J.* **2013**, *19*, 9606−9618.

(15) (a) Kochem, A.; Gellon, G.; Jarjayes, O.; Philouze, C.; Leconte, N.; van Gastel, M.; Bill, E.; Thomas, F. *Chem. Commun.* **2014**, *50*, 4924−4926. (b) Kochem, A.; Thomas, F.; Jarjayes, O.; Gellon, G.; Philouze, C.; Weyhermueller, T.; Neese, F.; van Gastel, M. *Inorg. Chem.* **2013**, *52*, 14428−14438. (c) Carrasco, R.; Cano, J.; Ottenwaelder, X.; Aukauloo, A.; Journaux, Y.; Ruiz-Garcia, R. *Dalton Trans.* **2005**, 2527−2538. (d) Cohen, C. T.; Thomas, C. M.; Peretti, K. L.; Lobkovsky, E. B.; Coates, G. W. *Dalton Trans.* **2006**, 237−249.

(e) Kemper, S.; Hrobarik, P.; Kaupp, M.; Schloerer, N. E. *J. Am. Chem. Soc.* **2009**, *131*, 4172−4172. (f) Vinck, E.; Murphy, D. M.; Fallis, I. A.; Strevens, R. R.; Van Doorslaer, S. *Inorg. Chem.* **2010**, *49*, 2083−2092.

(16) Eckshtain-Levi, M.; Orio, M.; Lavi, R.; Benisvy, L. *Dalton Trans.* **2013**, *42*, 13323−13326.

(17) (a) Ottenwaelder, X.; Aukauloo, A.; Journaux, Y.; Carrasco, R.; Cano, J.; Cervera, B.; Castro, I.; Curreli, S.; Munoz, M. C.; Rosello, A. L.; Soto, B.; Ruiz-Garcia, R. *Dalton Trans.* **2005**, 2516−2526. (b) Ottenwaelder, X.; Ruiz-Garcia, R.; Blondin, G.; Carasco, R.; Cano, J.; Lexa, D.; Journaux, Y.; Aukauloo, A. *Chem. Commun.* **2004**, 504−505.

(18) Jacobs, S. A.; Margerum, D. W. *Inorg. Chem.* **1984**, *23*, 1195−1201.

(19) (a) Bertz, S. H.; Cope, S.; Dorton, D.; Murphy, M.; Ogle, C. A. *Angew. Chem., Int. Ed.* **2007**, *46*, 7082−7085. (b) Bertz, S. H.; Cope, S.; Murphy, M.; Ogle, C. A.; Taylor, B. J. *J. Am. Chem. Soc.* **2007**, *129*, 7208−7208. (c) Hickman, A. J.; Sanford, M. S. *Nature* **2012**, *484*, 177−185. (d) Hu, H.; Snyder, J. P. *J. Am. Chem. Soc.* **2007**, *129*, 7210−7210. (e) Huffman, L. M.; Stahl, S. S. *J. Am. Chem. Soc.* **2008**, *130*, 9196−9196. (f) Ribas, X.; Jackson, D. A.; Donnadieu, B.; Mahia, J.; Parella, T.; Xifra, R.; Hedman, B.; Hodgson, K. O.; Llobet, A.; Stack, T. D. P. *Angew. Chem., Int. Ed.* **2002**, *41*, 2991−2994.

(20) (a) Citek, C.; Lin, B.-L.; Phelps, T. E.; Wasinger, E. C.; Stack, T. D. P. *J. Am. Chem. Soc.* **2014**, *136*, 14405−14408. (b) Cole, A. P.; Mahadevan, V.; Mirica, L. M.; Ottenwaelder, X.; Stack, T. D. P. *Inorg. Chem.* **2005**, *44*, 7345−7364. (c) DuBois, J. L.; Mukherjee, P.; Collier, A. M.; Mayer, J. M.; Solomon, E. I.; Hedman, B.; Stack, T. D. P.; Hodgson, K. O. *J. Am. Chem. Soc.* **1997**, *119*, 8578−8579. (d) DuBois, J. L.; Mukherjee, P.; Stack, T. D. P.; Hedman, B.; Solomon, E. I.; Hodgson, K. O. *J. Am. Chem. Soc.* **2000**, *122*, 5775−5787. (e) Henson, M. J.; Mukherjee, P.; Root, D. E.; Stack, T. D. P.; Solomon, E. I. *J. Am. Chem. Soc.* **1999**, *121*, 10332−10345. (f) Mahadevan, V.; DuBois, J. L.; Hedman, B.; Hodgson, K. O.; Stack, T. D. P. *J. Am. Chem. Soc.* **1999**, *121*, 5583−5584. (g) Root, D. E.; Henson, M. J.; Machonkin, T.; Mukherjee, P.; Stack, T. D. P.; Solomon, E. I. *J. Am. Chem. Soc.* **1998**, *120*, 4982−4990. (h) Itoh, S.; Taki, M.; Nakao, H.; Holland, P. L.; Tolman, W. B.; Que, L.; Fukuzumi, S. *Angew. Chem., Int. Ed.* **2000**, *39*, 398−398. (i) Mahapatra, S.; Halfen, J. A.; Wilkinson, E. C.; Pan, G. F.; Cramer, C. J.; Que, L.; Tolman, W. B. *J. Am. Chem. Soc.* **1995**, *117*, 8865−8866. (j) Mahapatra, S.; Young, V. G.; Kaderli, S.; Zuberbuhler, A. D.; Tolman, W. B. *Angew. Chem., Int. Ed.* **1997**, *36*, 130−133.

(21) Perrin, D. D.; Armarego, W. L. F. *Purification of Laboratory Chemicals,* 1st ed.; Pergamo Press: New York, 1988.

(22) Michel, F.; Hamman, S.; Philouze, C.; Del Valle, C. P.; Saint-Aman, E.; Thomas, F. *Dalton Trans.* **2009**, 832−842.

(23) (a) Connelly, N. G.; Geiger, W. E. *Chem. Rev.* **1996**, *96*, 877−910. (b) Steckhan, E. *Top. Curr. Chem.* **1987**, *142*, 1−69.

(24) (a) Bjorn, A. *A Mechanistic Investigation of the Photochemical and Thermal Activation of 2,2- and 2,3-Diaryl- and 2,2,3-Triaryl-2,3-dihydro-phenanthro[9,10-b]-1,4-dioxins, a New Class of 1,4-Dioxene Based DNA Cleaving Agents.* Ph.D. Thesis, University of Cincinnati, 2002. (b) Murata, Y.; Cheng, F.; Kitagawa, T.; Komatsu, K. *J. Am. Chem. Soc.* **2004**, *126*, 8874−8875.

(25) Noviandri, I.; Brown, K. N.; Fleming, D. S.; Gulyas, P. T.; Lay, P. A.; Masters, A. F.; Phillips, L. *J. Phys. Chem. B* **1999**, *103*, 6713−6722.

(26) SIR97; Altomare, A.; Burla, M. C.; Camalli, M.; Cascarano, G. L.; Giacovazzo, C.; Guagliardi, A.; Moliterni, A. G. G.; Polidori, G.; Spagna, R. *J. Appl. Crystallogr.,* **1999**, *32*, 115−119.

(27) Betteridge, P. W.; Carruthers, J. R.; Cooper, R. I.; Prout, K.; Watkin, D. J. *J. Appl. Crystallogr.* **2003**, *36*, 1487−1487.

(28) Huebschle, C. B.; Sheldrick, G. M.; Dittrich, B. *J. Appl. Crystallogr.* **2011**, *44*, 1281−1284.

(29) Frisch, M. J. et al. *Gaussian 09, Revision D.01;* Gaussian, Inc.: Wallingford, CT, 2009.

(30) (a) Becke, A. D. *J. Chem. Phys.* **1993**, *98*, 5648−5652. (b) Stephens, P. J.; Devlin, F. J.; Chabalowski, C. F.; Frisch, M. J. *J. Phys. Chem.* **1994**, *98*, 11623−11627.

(31) (a) Miertus, S.; Scrocco, E.; Tomasi, J. *Chem. Phys.* **1981**, *55*, 117−129. (b) Barone, V.; Cossi, M.; Tomasi, J. *J. Chem. Phys.* **1997**, *107*, 3210−3221. (c) Barone, V.; Cossi, M.; Tomasi, J. *J. Comput. Chem.* **1998**, *19*, 404−417. (d) Tomasi, J.; Mennucci, B.; Cances, E. *J. Mol. Struct.* **1999**, *464*, 211−226.

(32) (a) Schafer, A.; Huber, C.; Ahlrichs, R. *J. Chem. Phys.* **1994**, *100*, 5829−5835. (b) Schafer, A.; Horn, H.; Ahlrichs, R. *J. Chem. Phys.* **1992**, *97*, 2571−2577.

(33) (a) Casida, M. E. In *Recent Advances in Density Functional Methods*; Chong, D. P., Ed.; World Scientific: Singapore, 1995; p 155. (b) Stratmann, R. E.; Scuseria, G. E.; Frisch, M. J. *J. Chem. Phys.* **1998**, *109*, 8218−8224.

(34) (a) Tawada, Y.; Tsuneda, T.; Yanagisawa, S.; Yanai, T.; Hirao, K. *J. Chem. Phys.* **2004**, *120*, 8425−8433. (b) Yanai, T.; Tew, D. P.; Handy, N. C. *Chem. Phys. Lett.* **2004**, *393*, 51−57.

(35) (a) Becke, A. D. *Phys. Rev. A* **1988**, *38*, 3098−3100. (b) Lee, C. T.; Yang, W. T.; Parr, R. G. *Phys. Rev. B* **1988**, *37*, 785−789.

(36) (a) Gorelsky, S. I. *AOMix, Program for Molecular Orbital Analysis*; http://www.sg-chem.net/aomix/. (b) Gorelsky, S. I.; Lever, A. B. P. *J. Organomet. Chem.* **2001**, *635*, 187−196. (c) Gorelsky, S. I.; Solomon, E. I. *Theor. Chem. Acc.* **2008**, *119*, 57−67.

(37) Pratt, R. C.; Stack, T. D. P. *J. Am. Chem. Soc.* **2003**, *125*, 8716−8717.

(38) Dunn, T. J.; Webb, M. I.; Hazin, K.; Verma, P.; Wasinger, E. C.; Shimazaki, Y.; Storr, T. *Dalton Trans.* **2013**, *42*, 3950−3956.

(39) (a) Hansch, C.; Leo, A.; Taft, R. W. *Chem. Rev.* **1991**, *91*, 165−195. (b) Hewage, J. S.; Wanniarachchi, S.; Morin, T. J.; Liddle, B. J.; Banaszynski, M.; Lindeman, S. V.; Bennett, B.; Gardinier, J. R. *Inorg. Chem.* **2014**, *53*, 10070−10084. (c) Jovanovic, S. V.; Steenken, S. *J. Phys. Chem.* **1992**, *96*, 6674−6679. (d) Lever, A. B. P. *J. Porphyrins Phthalocyanines* **1999**, *3*, 488−499. (e) Masui, H.; Lever, A. B. P. *Inorg. Chem.* **1993**, *32*, 2199−2201.

(40) D'Alessandro, D. M.; Keene, F. R. *Chem. Soc. Rev.* **2006**, *35*, 424−440.

(41) (a) Hirotsu, M.; Kuwamura, N.; Kinoshita, I.; Kojima, M.; Yoshikawa, Y.; Ueno, K. *Dalton Trans.* **2009**, 7678−7683. (b) Jozwiuk, A.; Wang, Z. D.; Powell, D. R.; Houser, R. P. *Inorg. Chim. Acta* **2013**, *394*, 415−422. (c) Zolezzi, S.; Spodine, E.; Decinti, A. *Polyhedron* **2002**, *21*, 55−59.

(42) Robin, M. B.; Day, P. *Adv. Inorg. Chem. Radiochem.* **1967**, *10*, 247.

(43) Michel, F.; Hamman, S.; Thomas, F.; Philouze, C.; Gautier-Luneau, I.; Pierre, J. L. *Chem. Commun.* **2006**, 4122−4124.

(44) Lau, V. M.; Gorin, C. F.; Kanan, M. W. *Chem. Sci.* **2014**, *5*, 4975−4979.

(45) (a) Tedim, J.; Carneiro, A.; Bessada, R.; Patricio, S.; Magalhaes, A. L.; Freire, C.; Gurman, S. J.; Hillman, A. R. *J. Electroanal. Chem.* **2007**, *610*, 46−56. (b) Silva, A. R.; Freire, C.; de Castro, B.; Freitas, M. M. A.; Figueiredo, J. L. *Microporous Mesoporous Mater.* **2001**, *46*, 211−221.

(46) (a) Andreiadis, E. S.; Jacques, P.-A.; Tran, P. D.; Leyris, A.; Chavarot-Kerlidou, M.; Jousselme, B.; Matheron, M.; Pecaut, J.; Palacin, S.; Fontecave, M.; Artero, V. *Nat. Chem.* **2013**, *5*, 48−53. (b) Crist, B. V. The Elements and Native Oxides. In *Handbook of Monochromatic XPS Spectra*; XPS International: Mountain View, CA, 1999; Vol. *1*.

(47) The spin densities on the nickel center of $[\mathbf{Ni(Sal^R)}]^{+\bullet}$ when the CAM-B3LYP functional was used for optimization with no PCM model are as follows: R = CF$_3$: 25%; R = ^{t}Bu: 16%; R = OMe: 4%; R = NMe$_2$: 2%.

(48) Martin, R. L. *J. Chem. Phys.* **2003**, *118*, 4775−4777.

(49) (a) Bencini, A.; Fabbrizzi, L.; Poggi, A. *Inorg. Chem.* **1981**, *20*, 2544−2549. (b) Pinho, D.; Gomes, P.; Freire, C.; de Castro, B. *Eur. J. Inorg. Chem.* **2001**, 1483−1493.

(50) (a) Maki, A. H.; Davison, A.; Edelstein, N.; Holm, R. H. *J. Am. Chem. Soc.* **1964**, *86*, 4580−&. (b) Freire, C.; de Castro, B. *J. Chem. Soc., Dalton Trans.* **1998**, 1491−1497. (c) Azevedo, F.; Carrondo, M.; Decastro, B.; Convery, M.; Domingues, D.; Freire, C.; Duarte, M. T.; Nielsen, K.; Santos, I. C. *Inorg. Chim. Acta* **1994**, *219*, 43−54.

(51) Solomon, E. I.; Gorelsky, S. I.; Dey, A. *J. Comput. Chem.* **2006**, *27*, 1415−1428.